




Article

Isselite, $\text{Cu}_6(\text{SO}_4)(\text{OH})_{10}(\text{H}_2\text{O})_4 \cdot \text{H}_2\text{O}$, a new mineral species from Eastern Liguria, Italy

Cristian Biagioni^{1*} , Donato Belmonte², Cristina Carbone², Roberto Cabella², Nicola Demitri³, Natale Perchiazzi¹, Anthony R. Kampf⁴ and Ferdinando Bosi^{5,6}

¹Dipartimento di Scienze della Terra, Università di Pisa, Via Santa Maria 53, I-56126 Pisa, Italy; ²Dipartimento di Scienze della Terra, dell'Ambiente e della Vita (DISTAV), Università degli Studi di Genova, Corso Europa 26, I-16132 Genova, Italy; ³Elettra – Sincrotrone Trieste S.C.p.A., S.S. 14 km 163,5 in Area Science Park, Basovizza, I-34149 Trieste, Italy; ⁴Mineral Sciences Department, Natural History Museum of Los Angeles County, 900 Exposition Boulevard, Los Angeles, CA 90007, USA; ⁵Dipartimento di Scienze della Terra, Sapienza Università di Roma, Piazzale Aldo Moro 5, 00185 Rome, Italy; and ⁶CNR-Istituto di Geologia Ambientale e Geoingegneria, Sede Secondaria di Roma “Sapienza”, Piazzale Aldo Moro 5, I-00185 Roma, Italy

Abstract

The new mineral isselite, $\text{Cu}_6(\text{SO}_4)(\text{OH})_{10}(\text{H}_2\text{O})_4 \cdot \text{H}_2\text{O}$, has been discovered in the Lagoscuro mine, Monte Ramazzo mining complex, Genoa, Eastern Liguria, Italy. It occurs as sprays of blue acicular crystals, up to 0.1 mm long, associated with brochantite and posnjakite. Streak is light blue and the lustre is vitreous. Isselite is brittle, with irregular fracture and good cleavage on {001} and {100}. Measured density is 3.00(2) g/cm³. Isselite is optically biaxial (–), with $\alpha = 1.599(2)$, $\beta = 1.633(2)$ and $\gamma = 1.647(2)$ (determined in white light). The measured 2V is 63.6(5)°. Dispersion is moderate, with $r > v$. The optical orientation is $X = \mathbf{b}$, $Y = \mathbf{c}$ and $Z = \mathbf{a}$. Isselite is pleochroic, with $X = \text{light blue}$, $Y = \text{blue}$, $Z = \text{blue}$; $X \ll Z < Y$. Electron microprobe analyses give (wt.%): SO₃ 11.45(21), MgO 0.31(7), CoO 1.07(14), NiO 9.41(90), CuO 51.29(126), ZnO 1.10(20), H₂O_{calc} 24.21, total 98.84. The empirical formula of isselite, based on $\Sigma(\text{Mg}, \text{Co}, \text{Ni}, \text{Cu}, \text{Zn}) = 6$ atoms per formula unit, is $(\text{Cu}_{4.80}\text{Ni}_{0.94}\text{Co}_{0.11}\text{Zn}_{0.10}\text{Mg}_{0.06})_{\Sigma 6.00}(\text{S}_{1.06}\text{O}_{4.19})(\text{OH})_{10} \cdot 5\text{H}_2\text{O}$. Isselite is orthorhombic, space group $Pmn2_1$, with unit-cell parameters $a = 6.8070(14)$, $b = 5.8970(12)$, $c = 20.653(4)$ Å, $V = 829.0(3)$ Å³ and $Z = 2$. The crystal structure of isselite was refined from single-crystal X-ray diffraction data to $R_1 = 0.067$ on the basis of 2964 reflections with $F_o > 4\sigma(F_o)$. It shows a layered structure formed by zig-zag {001} layers of Cu-centred polyhedra. Sulfate groups occur in the interlayer along with one H₂O group. Isselite is chemically related to redgillite and montetrisaite.

Keywords: isselite, new mineral species, sulfate, copper, crystal structure, Monte Ramazzo mining complex, Eastern Liguria, Italy

(Received 11 March 2020; accepted 15 June 2020; Accepted Manuscript published online: 19 June 2020; Associate Editor: David Hibbs)

Introduction

The ore deposits of Eastern Liguria, Northern Apennines, Italy, are well-known among mineralogists for the occurrence of several rare species from the Mn ore deposits hosted in middle Jurassic metacherts of the Graveglia Valley, Genoa Province (Cabella *et al.*, 1998; Bindi *et al.*, 2013; Biagioni *et al.*, 2019a) and the Cerchiara Mine, La Spezia Province (Kampf *et al.*, 2013; Kolitsch *et al.*, 2018). In addition, Cu–Fe–Ni–Co sulfide ore deposits are also hosted in ophiolitic rocks of the Northern Apennines and the Sestri–Votaggio Zone, where several types of Volcanic Massive Sulfide (VMS) deposits occur in mafic–ultramafic rocks at different stratigraphic positions within the ophiolitic sequences (Ferrario and Garuti, 1980; Zaccarini and Garuti, 2008; Schwarzenbach *et al.*, 2012). Among them, stockwork-vein and seafloor stratiform orebodies are associated with serpentinised mantle peridotites and serpentinite breccias (e.g. Ferrario and Garuti, 1980), like in the Monte Ramazzo–

Lagoscuro area, where a pyrrhotite-dominated mineralisation had been actively exploited since the beginning of the 19th Century (Rolandi, 1974; Pipino, 1977). The primary mineralisation underwent subsequent fluid–rock interaction, hydrothermal mobilisation, and multi-stage alteration processes which led, on the one hand, to sulfide reconcentration and recrystallisation along tectonic structures, on the other hand to metal reworking and the formation of secondary phases, such as (Ni,Co)-bearing oxy-hydroxides (asbolane and heterogenite), carbonates (kolwezite, Co-rich malachite and spherocobaltite) and silicates (pecoraite). This peculiar mineral assemblage occurring in the Monte Ramazzo–Lagoscuro ore deposit is quite different from other hydrothermal sulfide mineralisation described so far in ophiolites from the Eastern Liguria, where (Ni,Co)-enrichment occurs mostly in pyrite and/or accessory minerals like millerite, siegenite and pentlandite (e.g. Cortesogno *et al.*, 1977; Schwarzenbach *et al.*, 2012; Moroni *et al.*, 2019).

During the examination of secondary minerals from the Monte Ramazzo mining complex, blue acicular crystals from the Lagoscuro mine were encountered. Crystallographic studies and chemical analyses showed this phase to be a new mineral species, which we describe herein and name isselite. The mineral and its name have been approved by the International Mineralogical

*Author for correspondence: Cristian Biagioni, Email: cristian.biagioni@unipi.it

Cite this article: Biagioni C., Belmonte D., Carbone C., Cabella R., Demitri N., Perchiazzi N., Kampf A.R. and Bosi F. (2020) Isselite, $\text{Cu}_6(\text{SO}_4)(\text{OH})_{10}(\text{H}_2\text{O})_4 \cdot \text{H}_2\text{O}$, a new mineral species from Eastern Liguria, Italy. *Mineralogical Magazine* 84, 653–661. <https://doi.org/10.1180/mgm.2020.50>

Association (IMA) Commission on New Minerals, Nomenclature and Classification (CNMNC) (IMA2018-139, Biagioni *et al.*, 2019b). Holotype material for isselite is deposited in the mineralogical collection of the Museo di Storia Naturale, Università di Pisa, Via Roma 79, Calci, Pisa, Italy, under catalogue number 19904, and of the Dipartimento di Scienze della Terra, dell'Ambiente e della Vita (DISTAV), Università di Genova, Corso Europa 26, Genova, Italy, under catalogue number MO484. Cotype material is preserved in the collections of the Natural History Museum of Los Angeles County, 900 Exposition Boulevard, Los Angeles, CA 90007, USA, catalogue number 67195. The new mineral is dedicated to Arturo Issel (1842–1922) for his pioneering work on the geology, palaeontology and mineralogy of Italy, with a special reference to Liguria (Issel, 1892). He was professor of Geology and Mineralogy at the University of Genoa beginning in 1866 and Director of the Institute of Geology and the Geological Museum until 1917. Arturo Issel was the author of important scientific monographs on a variety of topics (not only geology and palaeontology, but also anthropology and ethnology) and contributed to several geological maps of Liguria.

Occurrence and physical properties

Isselite occurs as a secondary phase in the Fe–Ni–Co sulfide mineralisation formerly exploited at the Lagoscuro mine (44°28'35"N, 8°51'35"E), Ceranesi, Genoa Province, Liguria, Italy. This mine, which belongs to the Monte Ramazzo mining complex, operated from 1815 to 1825, mainly for magnesium sulfate (Pipino, 1977). The Co-rich pyrrhotite + pentlandite ± sphalerite sulfide ore, hosted within serpentinite and serpentinite breccia in contact with basaltic rocks belonging to the Figogna Unit in the Ligurian Alps (Galli, 1954 and 1963; Capponi and Crispini, 2008), underwent multi-stage alteration processes and hydrothermal mobilisation, which developed a mineral assemblage formed by violarite + valleriite + andradite ± magnetite, along with other Ni–Co secondary minerals (e.g. pecoraite, heterogenite and asbolane) and hydrated Mg–Cu(–Ni) carbonates and sulfates such as malachite, brochantite, langite, posnjakite and hydromagnesite. The transformation of pentlandite to violarite in the sulfide ore seems to constrain the first stage of hydrothermal alteration to $T < 210^\circ\text{C}$ under strongly acidic to neutral (i.e. $1 < \text{pH} < 6$) and reducing (i.e. $\log f_{\text{O}_2(\text{g})} < -35$) conditions (Tenailleau *et al.*, 2006; Xia *et al.*, 2009).

Isselite was identified in only a few specimens as sprays of blue acicular crystals, striated parallel to [100] and tabular on {001}, up to 0.1 mm long (Fig. 1). Observed forms are {001}, {010}, {103} and {10 $\bar{3}$ }. The streak is light blue. Isselite is vitreous and transparent. The mineral is brittle, with an irregular fracture and good cleavage on {001} and {100}. Hardness was not measured, owing to the small crystal size. The density measured by sink–float in methylene iodine – toluene is 3.00(2) g/cm³, compared with a density of 2.946 g/cm³, calculated on the basis of the empirical formula and the unit-cell volume refined from single-crystal X-ray diffraction data at room temperature.

Isselite is optically biaxial (–), with indices of refraction $\alpha = 1.599(2)$, $\beta = 1.633(2)$ and $\gamma = 1.647(2)$ (determined in white light). The measured $2V$ of 63.6(5)°, obtained using extinction data analysed with EXCALIBUR (Gunter *et al.*, 2004), compares well with the calculated $2V$ of 64.2°. Dispersion is moderate, with $r > v$. The optical orientation is $X = \mathbf{b}$, $Y = \mathbf{c}$ and $Z = \mathbf{a}$. Isselite is pleochroic, with $X = \text{light blue}$, $Y = \text{blue}$; $X \ll Z < Y$. The compatibility index, calculated using the Gladstone–Dale



Fig. 1. Isselite, sprays of acicular blue crystals. Field of view: 2 mm. Monte Ramazzo mining complex, Genoa. Photo M. Esposito. The crystal morphology is shown to the right.

Table 1. Electron microprobe analysis of isselite (average of six spot analyses – in wt.%).

Oxide	Mean	Range	S.D.
SO ₃	11.45	11.30–11.73	0.21
MgO	0.31	0.20–0.40	0.07
CoO	1.07	0.89–1.22	0.14
NiO	9.41	8.63–11.01	0.90
CuO	51.29	49.03–52.55	1.26
ZnO	1.10	0.86–1.42	0.20
H ₂ O _{calc}	24.21		
Total	98.84		

S.D. – standard deviation

relationship (Mandarino, 1979, 1981), is 0.003 (superior), using the empirical formula and the calculated density; it is 0.021 (excellent) using the empirical formula and the measured density.

Isselite is a late-stage, secondary mineral that crystallised from a low-temperature, aqueous solution. In holotype material, it is associated closely with brochantite and posnjakite. Other associated minerals are pyrrhotite, pentlandite, allophane, chrysocolla and langite. The source of the Cu in isselite may be valleriite, along with minor chalcopyrite, covellite and digenite. These sulfides are widespread in the Monte Ramazzo–Lagoscuro ore deposit, though not in close association with isselite in the samples studied.

Chemical and spectroscopic analyses

Preliminary energy-dispersive spectroscopy (EDS) chemical analyses showed that isselite contains Cu, Ni, Co and S as the only elements with $Z > 8$. Quantitative chemical analyses were performed using a CAMECA SX50 electron microprobe (Istituto di Geologia Ambientale e Geoingegneria, CNR, Rome) operating in wave-length dispersive mode. Operating conditions were: accelerating voltage 15 kV, beam current 15 nA, and beam diameter 5 μm. Standards (element, emission line) were: periclase (MgKα), baryte (SKα), synthetic Co (CoKα), synthetic Ni (NiKα), synthetic Cu (CuKα) and synthetic Zn (ZnKα). Iron and Pb were sought but found to be below detection limits. The small amount of available material precluded the determination of H₂O by direct measurement; consequently, the H₂O content was inferred from the crystal structure analysis. Its presence is confirmed by Raman spectroscopy (see below).

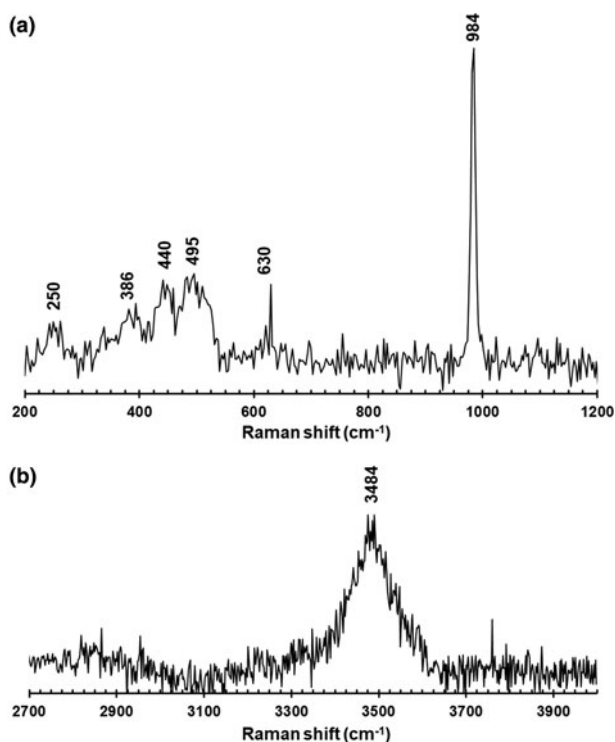


Fig. 2. Raman spectrum of isselite in the range 200–1200 cm^{-1} (a) and 2700–4000 cm^{-1} (b).

The electron microprobe analysis results are given in Table 1. The empirical formula of isselite, based on $\Sigma(\text{Mg}, \text{Co}, \text{Ni}, \text{Cu}, \text{Zn}) = 6$ atoms per formula unit, is $(\text{Cu}_{4.80}\text{Ni}_{0.94}\text{Co}_{0.11}\text{Zn}_{0.10}\text{Mg}_{0.06})_{\Sigma 6.00}(\text{S}_{1.06}\text{O}_{4.19})(\text{OH})_{10}\cdot 5\text{H}_2\text{O}$. The ideal formula of isselite is $\text{Cu}_6(\text{SO}_4)(\text{OH})_{10}\cdot 5\text{H}_2\text{O}$, which requires SO_3 10.86, CuO 64.71, H_2O 24.43, total 100.00.

Micro-Raman spectra were obtained on an unpolished sample of isselite in nearly back-scattered geometry with a Jobin-Yvon Horiba XploRA Plus apparatus, equipped with a motorised x - y stage and an Olympus BX41 microscope with a 10 \times objective (Dipartimento di Scienze della Terra, Università di Pisa). The 532 nm line of a solid-state laser was used. The minimum lateral and depth resolution was set to a few μm . The system was calibrated using the 520.6 cm^{-1} Raman band of silicon before each experimental session. Spectra were collected through multiple acquisitions with single counting times of 60 s. Back-scattered radiation was analysed with a 1200 gr/mm grating monochromator. The Raman spectrum of isselite is shown in Fig. 2. The strongest band occurs at 984 cm^{-1} and can be related to the symmetrical stretching ν_1 of the SO_4 group. The bands at 386, 440 and 495 cm^{-1} can be interpreted as due to the symmetrical bending ν_2 of the SO_4 group, whereas the weak band at 630 cm^{-1} could be related to the antisymmetrical bending ν_4 . Finally, the band at 250 cm^{-1} may be attributed to lattice modes. The broad band at 3484 cm^{-1} can be attributed to the O–H stretching modes. No evident bending of H–O–H bonds, in the typical range between 1595–1700 cm^{-1} (e.g. Kolesov,

Table 2. X-ray powder diffraction (d in \AA) data for isselite.*

l_{obs}	d_{obs}	l_{calc}	d_{calc}	hkl
s	10.3	92	10.3	0 0 2
m	6.4	29	6.46	1 0 1
mw	5.67	25	5.67	0 1 1
w	5.14	11	5.12	0 1 2
vs	4.84	100	4.84	1 0 3
vw	4.47	9	4.48	0 1 3
vw	4.32	4	4.36	1 1 1
vw	4.14	1	4.09	1 1 2
w	3.742	7	3.741	1 1 3
vw	3.462	4	3.442	0 0 6
mw	3.400	8, 11	3.404, 3.383	2 0 0, 0 1 5
vw	3.237	4	3.232	2 0 2
vw	3.035	4	3.029	1 1 5
w	2.919	7	2.918	2 1 1
w	2.838	10	2.842	2 0 4
s	2.708	4, 16, 22, 14, 12	2.710, 2.710, 2.708, 2.706, 2.683	0 2 3, 2 1 3, 1 0 7, 1 2 0, 1 2 1
vw	2.628	3	2.638	0 1 7
w	2.589	10	2.582	0 0 8
vw	2.516	3	2.518	1 2 3
w	2.406	6	2.420	2 0 6
m	2.225	5, 13	2.229, 2.216	2 2 0, 2 2 1
mw	2.179	11	2.178	2 2 2
mw	2.129	7	2.120	2 2 3
mw	2.065	10	2.065	0 0 10
w	2.044	2, 1	2.046, 2.040	2 2 4, 1 1 9
w	1.943	2	1.931	0 3 2
vw	1.886	2, 1	1.871, 1.868	2 2 6, 1 2 8
mw	1.796	2, 2, 5, 6, 6	1.810, 1.799, 1.798, 1.791, 1.778	1 0 11, 3 0 7, 3 2 0, 3 2 1, 2 2 7
mw	1.701	6	1.698	4 0 0
		3	1.698	3 2 4
		6	1.687	2 2 8

*Notes: the d_{hkl} values were calculated on the basis of the unit cell refined by using single-crystal data. Intensities were calculated on the basis of the structural model reported in Table 4. Observed intensities were visually estimated: vs = very strong; s = strong; m = medium; mw = medium-weak; w = weak; vw = very weak. Only reflections with $l_{\text{calc}} > 5$ are listed, if not observed. The strongest reflections are shown in bold.

Table 3. Crystal data and summary of parameters describing data collection and refinement for isselite.

Crystal data	
Crystal size (mm)	0.080 × 0.010 × 0.005
Cell setting, space group	Orthorhombic, <i>Pmn</i> 2 ₁
<i>a</i> (Å)	6.8070(14)
<i>b</i> (Å)	5.8970(12)
<i>c</i> (Å)	20.653(4)
<i>V</i> (Å ³)	829.0(3)
<i>Z</i>	2
Data collection	
Radiation, wavelength (Å)	Synchrotron, 0.59040
Temperature (K)	298(2)
2θ _{max} (°)	59.46
Measured reflections	18,207
Unique reflections	4088
Reflections with <i>F</i> _o > 4σ(<i>F</i> _o)	2964
<i>R</i> _{int}	0.0651
<i>R</i> σ	0.0488
Range of <i>h</i> , <i>k</i> , <i>l</i>	−9 ≤ <i>h</i> ≤ 10, −9 ≤ <i>k</i> ≤ 9, −34 ≤ <i>l</i> ≤ 34
Refinement	
<i>R</i> [<i>F</i> _o > 4σ(<i>F</i> _o)]	0.0669
<i>R</i> (all data)	0.0921
<i>wR</i> (on <i>F</i> _o)	0.1790
Gof	1.013
Number of least-squares parameters	140
Δ <i>p</i> _{max} , Δ <i>p</i> _{min} (e [−] /Å ³)	6.19 [at 1.31 Å from O(3)] −1.38 [at 0.67 Å from Cu(4)]

2006), was observed. The interpretation of the spectral bands is in agreement with Frost *et al.* (2004).

Crystallography

The powder X-ray diffraction pattern of isselite was obtained using a 114.6 mm diameter Gandolfi camera, with Ni-filtered CuKα radiation. The observed powder X-ray diffraction pattern is compared with the calculated one (obtained using the software *PowderCell*; Kraus and Nolze, 1996) in Table 2. Unit-cell parameters, refined from the powder data on the basis of 22 unequivocally indexed reflections through the software *UnitCell* (Holland and Redfern, 1997), are *a* = 6.789(1), *b* = 5.923(1), *c* = 20.651(3) Å, *V* = 830.4(2) Å³ and *Z* = 2.

The single-crystal X-ray diffraction study was carried out at the XRD1 beamline, ELETTRA synchrotron facility (Lausi *et al.*, 2015). A monochromatic wavelength of 0.59040 Å was used on a 50 μm × 50 μm beam size, using a Dectris Pilatus 2M hybrid pixel area detector at a distance of 85 mm. A total of 500 frames was collected using φ scan mode in Δφ = 0.5° slices, with an exposure time of 1 s per frame. The diffraction data, collected at room temperature, were indexed, integrated, scaled, and corrected for the Lorentz-polarisation factor using the software *XDS* (Kabsch, 2010). The refined unit-cell parameters are *a* = 6.8070(14), *b* = 5.8970(12), *c* = 20.653(4) Å and *V* = 829.0(3) Å³. The *a*:*b*:*c* ratio calculated from unit-cell parameters is 1.1543:1.3:5.023.

The statistical tests on the distribution of $|E|$ values ($|E^2 - 1| = 0.703$) suggest the acentric nature of isselite. The examination of the systematic absences indicated the possible space groups *P2*₁*nm* and *Pmn*2₁. Only the choice of this latter space group allowed the solution of the crystal structure through direct methods using *Shelxs-97* (Sheldrick, 1997). After having located the heavier elements, the structure was completed through successive difference-Fourier maps; owing to the quality of available material, H atoms were not located. After several cycles of anisotropic refinement, performed using *Shelxl-2018* (Sheldrick, 2015) and using

Table 4. Sites, Wyckoff positions, atom coordinates and equivalent isotropic displacement parameters (Å²) for isselite.

Site	Wyk.	<i>x</i>	<i>y</i>	<i>z</i>	<i>U</i> _{eq}
Cu(1)	2 <i>a</i>	0	0.0315(3)	0.01412(8)	0.0249(4)
Cu(2)	2 <i>a</i>	0	0.5234(3)	0.00062(8)	0.0239(4)
Cu(3)	2 <i>b</i>	½	0.8539(3)	0.22094(7)	0.0228(3)
Cu(4)	4 <i>c</i>	0.24886(18)	0.68698(18)	0.11180(8)	0.0230(2)
Cu(5)	2 <i>b</i>	½	0.3447(3)	0.20795(8)	0.0227(3)
S	2 <i>b</i>	½	0.9276(7)	0.88577(19)	0.0345(7)
OH(1)	2 <i>b</i>	½	0.8412(17)	0.1134(7)	0.028(2)
OH(2)	2 <i>a</i>	0	0.5310(16)	0.1093(7)	0.0264(18)
OH(3)	4 <i>c</i>	0.3117(10)	0.5960(11)	0.2008(4)	0.0237(12)
OH(4)	4 <i>c</i>	0.3064(11)	0.1076(12)	0.2213(4)	0.0268(14)
OH(5)	4 <i>c</i>	0.1864(11)	0.7802(11)	0.0236(4)	0.0242(13)
OH(6)	4 <i>c</i>	0.1940(12)	0.2701(12)	0.0003(4)	0.0288(14)
Ow(7)	2 <i>b</i>	½	0.804(3)	0.3252(9)	0.054(4)
Ow(8)	2 <i>a</i>	0	0.612(3)	0.8958(9)	0.054(4)
O(9)	2 <i>b</i>	½	0.814(3)	0.9481(7)	0.041(3)
O(10)	2 <i>b</i>	½	0.172(2)	0.8931(8)	0.059(4)
O(11)	4 <i>c</i>	0.328(3)	0.858(3)	0.8504(8)	0.096(6)
Ow(12)	2 <i>a</i>	0	0.067(2)	0.1407(6)	0.034(2)
Ow(13)	2 <i>b</i>	½	0.306(2)	0.0840(6)	0.036(2)
Ow(14)	2 <i>a</i>	0	0.563(2)	0.2837(6)	0.037(2)

Wyk. = Wyckoff position

Table 5. Selected bond distances (in Å) for isselite.

Cu(1)–OH(6)	1.950(8) × 2	Cu(4)–OH(2)	1.928(5)
Cu(1)–OH(5)	1.961(7) × 2	Cu(4)–OH(1)	1.937(5)
<Cu(1)–OH>	1.956	Cu(4)–OH(5)	1.950(7)
Cu(1)–Ow(12)	2.623(13)	Cu(4)–OH(3)	1.963(7)
		<Cu(4)–OH>	1.944
Cu(2)–OH(6)	1.994(8) × 2	Cu(4)–Ow(12)	2.871(11)
Cu(2)–OH(5)	2.032(7) × 2	Cu(4)–Ow(13)	2.883(10)
Cu(2)–Ow(8)	2.23(2)		
Cu(2)–OH(2)	2.244(14)	Cu(5)–OH(4)	1.941(7) × 2
<Cu(2)–OH>	2.088	Cu(5)–OH(3)	1.965(7) × 2
		<Cu(5)–OH>	1.953
Cu(3)–OH(4)	1.994(7) × 2	Cu(5)–Ow(13)	2.571(13)
Cu(3)–OH(3)	2.032(7) × 2		
Cu(3)–Ow(7)	2.173(18)	S–O(11)	1.441(13) × 2
Cu(3)–OH(1)	2.222(14)	S–O(10)	1.448(12)
<Cu(3)–OH>	2.074	S–O(9)	1.452(14)
		<S–O>	1.446

neutral scattering curves taken from the *International Tables for Crystallography* (Wilson, 1992), the refinement converged to *R*₁ = 0.0669 for 2964 unique reflections with *F*_o > 4σ(*F*_o) and 140 refined parameters. The occurrence of high electron density residuals (up to 6.19 e[−]/Å³) is related to the less-than-ideal quality of the available crystals of isselite. An attenuation of the residuals can be obtained by truncating the intensity data to low angular values. For instance, the truncation of the dataset to 30° in 2θ results in a highest residual of 2.3 e[−]/Å³. However, the ratio between observed reflections and least-square parameters significantly decreases (from ~21 to ~4.5). An attempt at truncating the dataset at 2θ = 50° resulted in a slightly better *R* value (0.0625 for 2269 reflections) and slightly lower residuals (up to 5.4 e[−]/Å³). However, the estimated standard uncertainties on bond lengths slightly increased. For this reason, the full dataset is here presented, with the awareness of the non ideal quality of the structure refinement (in particular as regards the high residuals) but supported by the crystal-chemical soundness of the proposed structural model.

Details of the data collection and crystal-structure refinement are given in Table 3. Atom coordinates and equivalent isotropic

Table 6. Bond-valence sums (BVS – in valence units) for isselite*.

	Cu(1)	Cu(2)	Cu(3)	Cu(4)	Cu(5)	S	Σ anions
OH(1)			0.23	$2^{\times-}0.50$			1.23
OH(2)		0.22		$2^{\times-}0.51$			1.24
OH(3)			$0.39^{1 \times 2}$	0.46	$0.46^{1 \times 2}$		1.31
OH(4)			$0.43^{1 \times 2}$		$0.49^{1 \times 2}$		0.92
OH(5)	$0.47^{1 \times 2}$	$0.39^{1 \times 2}$		0.48			1.34
OH(6)	$0.48^{1 \times 2}$	$0.43^{1 \times 2}$					0.91
Ow(7)			0.26				0.26
Ow(8)		0.23					0.23
O(9)						1.59	1.59
O(10)						1.61	1.61
O(11)						$1.64^{1 \times 2}$	1.64
Ow(12)	0.08			$2^{\times-}0.04$			0.16
Ow(13)				$2^{\times-}0.04$	0.09		0.17
Ow(14)							–
Σ cations	1.98	2.09	2.13	2.03	1.99	6.48	
Theoretical	2.00	2.00	2.00	2.00	2.00	6.00	

*Left and right superscripts indicate the number of equivalent bonds involving anions and cations, respectively.

displacement parameters are reported in Table 4, whereas Table 5 gives selected bond distances. Bond-valence calculations, shown in Table 6, were performed using the bond parameters of Brese and O’Keeffe (1991). The crystallographic information file has been deposited with the Principal Editor of *Mineralogical Magazine* and is available as Supplementary material (see below).

Crystal structure description

General organisation

The crystal structure of isselite (Fig. 3) includes five independent Cu sites, one S site, and fourteen O positions. It can be described as formed by {001} zig-zag layers of $\text{Cu}\Phi_{4-6}$ polyhedra, where $\Phi = (\text{OH} \text{ or } \text{H}_2\text{O})$. Sulfate groups occur in the interlayer, together with one H_2O group. No H positions were located from the structure determination; the assignments of OH and H_2O groups were based on the bond-valence analysis (see Table 6).

Cation coordination and site occupancies

In isselite, the Cu sites display different kinds of coordination (Fig. 4). The Cu(2) and Cu(3) sites show the typically distorted (4 + 2) octahedral coordination of Cu^{2+} , related to the Jahn-Teller effect (e.g. Burns and Hawthorne, 1996). The average value of the four shorter distances is 2.013 Å for both sites, somewhat longer than the equatorial bond length of 1.97 Å reported by Eby and Hawthorne (1993). The two apical Cu–O distances have average values of 2.237 and 2.197 Å at the Cu(2) and Cu(3) sites, respectively, shorter than the average value of 2.44 Å reported by Eby and Hawthorne (1993). The smaller than typical octahedral distortions observed for the Cu(2) and Cu(3) sites suggest that minor Ni and Co detected in isselite are located at these two sites. Taking into account the nature of the ligands, Cu(2) and Cu(3) octahedra can be defined both as $\text{Cu}(\text{OH})_5(\text{H}_2\text{O})$ polyhedra. The Cu(1) and Cu(5) sites have a square pyramidal coordination, with four equatorial bonds ranging between 1.941 and 1.965 Å (average value of 1.954 Å); the fifth bond is at a longer distance, i.e. 2.571 Å [Cu(5)–Ow(13)] and 2.623 Å [Cu(1)–Ow(12)]. Taking into account the ligand nature, the cations at the Cu(1) and Cu(5) sites can be related to the $\text{Cu}(\text{OH})_4(\text{H}_2\text{O})$ polyhedra.

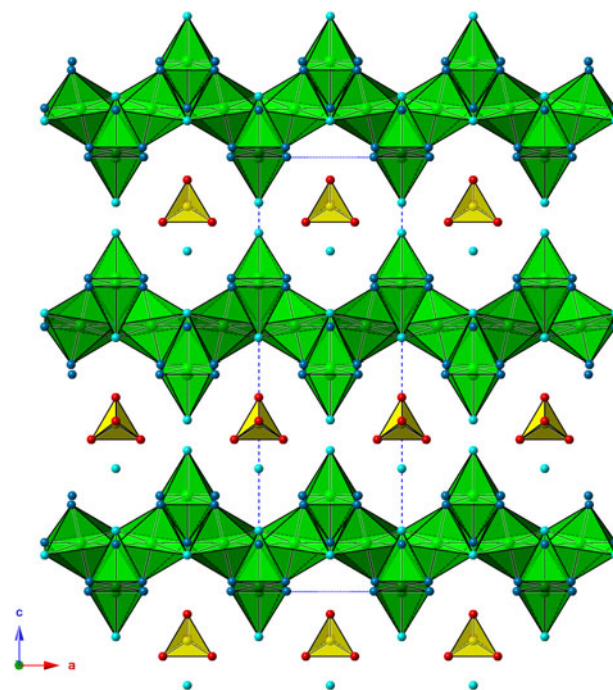


Fig. 3. Crystal structure of isselite as seen down **b**. Symbols: green polyhedra = Cu sites and yellow polyhedra = S site. Circles: red = O^{2-} , blue = OH^- and light blue = H_2O .

A square-planar coordination is shown by the Cu(4) site, having four ligands at an average distance of 1.944 Å, in agreement with the ideal mean value of 1.94 Å for square-planar Cu^{2+} (Eby and Hawthorne, 1993). Taking into account the two very long distances Cu(4)–Ow(12) and Cu(4)–Ow(13), ≈ 2.9 Å, a very distorted octahedron $\text{Cu}(\text{OH})_4(\text{H}_2\text{O})_2$ can be identified, instead of a square-planar group $\text{Cu}(\text{OH})_4$.

Bond-valence sums (BVS) at the Cu sites range between 1.98 and 2.13 valence units (vu), in agreement with the occurrence of Cu in the divalent state. The higher values occur at the Cu(2) and Cu(3) sites and can be related to the admixture of minor Ni^{2+} and very small amounts of Co^{2+} , Zn^{2+} and Mg^{2+} .

The SO_4 group is hosted in the interlayer and is bonded to the {001} Cu layers through hydrogen bonds, as revealed by the occurrence of several underbonded O in the bond-valence calculation (Table 6) and the occurrence of short O...O distances (Table 7). The BVS at the S site is 6.48 vu, considerably greater than expected for S^{6+} . In this regard, it should be noted that the position of O(11) seems to be affected by disorder, as indicated by a U_{eq} value larger than those of other O atoms belonging to the SO_4 group.

Hydrogen bonds

The short O...O distances are given in Table 7, confirming the importance of H bonds in the crystal structure of isselite, in agreement with the undersaturation of all O atoms. Taking into account the results of BVS given in Table 6, three distinct groups of O atoms can be found: (1) O atoms having BVS close to ~ 1.6 vu; (2) O atoms with BVS of ~ 1.2 – 1.3 vu; and (3) O atoms showing BVS of ~ 0.2 vu. These three different O groups correspond to O^{2-} , $(\text{OH})^-$ and H_2O groups, respectively.

Oxygen atoms belonging to the isolated SO_4 groups, that is O(9), O(10) and O(11), are acceptors of H bonds. Oxygen atom

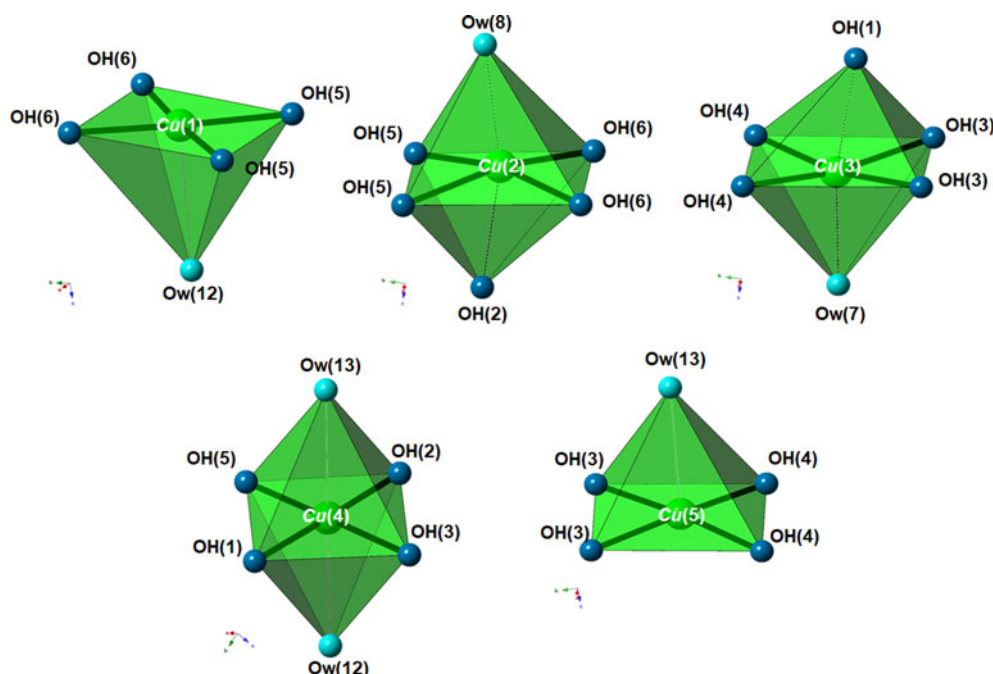


Fig. 4. Coordination environments of Cu^{2+} in the crystal structure of isselite. The colour scheme is the same as in Fig. 3.

hosted at O(9) is an acceptor of two H bonds from two symmetry-related $(\text{OH})^-$ groups hosted at OH(5); the oxygen atom at O(10) is an acceptor of H bonds from two symmetry-related $(\text{OH})^-$ groups hosted at OH(6) and from an H_2O group occurring at the Ow(14) site. Finally, O(11) is involved in a more complex H-bond system. Indeed, O(11) is an acceptor of H bonds from OH(4) and it is at H-bond distances with Ow(7), Ow(8), and Ow(14). In addition, Ow(14) is an acceptor of H bonds from two symmetry-related OH(3) groups, whereas a still more complex situation involves the H_2O groups hosted at Ow(7) and Ow(8). These two H_2O groups are bonded to the Cu atoms hosted at Cu(3) and Cu(2) sites, respectively. Both are at short O...O distances with O(11). In addition, the distance Ow(7)...Ow(8), 2.85 Å, suggests another H-bond contact. Owing to the lack of knowledge about the H positions and the occurrence of different possible configurations, the actual H-bond system involving these atoms has to be considered only speculative and it will not be detailed here. As a matter of fact, the possibility of different configurations involving the oxygen atom hosted at O(11) could be the reason for its relatively high U_{eq} value. Its position could be an average position between different H-bond configurations. Moreover, this uncertainty could affect the BVS of S, as discussed briefly above.

Oxygen atoms hosted at OH(4) and OH(6) are both donor (in the H bonds described above) and acceptor from H_2O groups hosted at Ow(12) and Ow(13), respectively. It is worth noting that Ow(12) and Ow(13) act as donor to two symmetry-related OH(4) and OH(6), respectively, whereas they are acceptors of H bonds from OH(2) and OH(1), respectively.

Discussion

Isselite and relations with other Cu sulfates

Fifteen different mineral species are currently known in the system $\text{CuO-SO}_3\text{-H}_2\text{O}$ (Table 8). From a chemical point of view,

Table 7. O...O distances (in Å) and corresponding bond strengths (in valence units, vu*).

O...O	<i>d</i> (Å)	vu*
OH(1)...Ow(13)	2.805(15)	0.18
OH(2)...Ow(12)	2.813(15)	0.18
OH(3)...Ow(14)	2.733(11)	0.21
OH(4)...O(11)	2.825(16)	0.17
Ow(12)...OH(4)	2.679(12)	0.24
OH(5)...O(9)	2.650(11)	0.25
OH(6)...O(10)	3.094(14)	0.11
Ow(13)...OH(6)	2.714(12)	0.22
Ow(7)...Ow(8)	2.85(2)	0.17
Ow(7)...O(11)	3.04(2)	0.12
Ow(8)...O(11)	2.82(2)	0.18
Ow(14)...O(10)	2.75(2)	0.20
Ow(14)...O(11)	3.07(2)	0.12

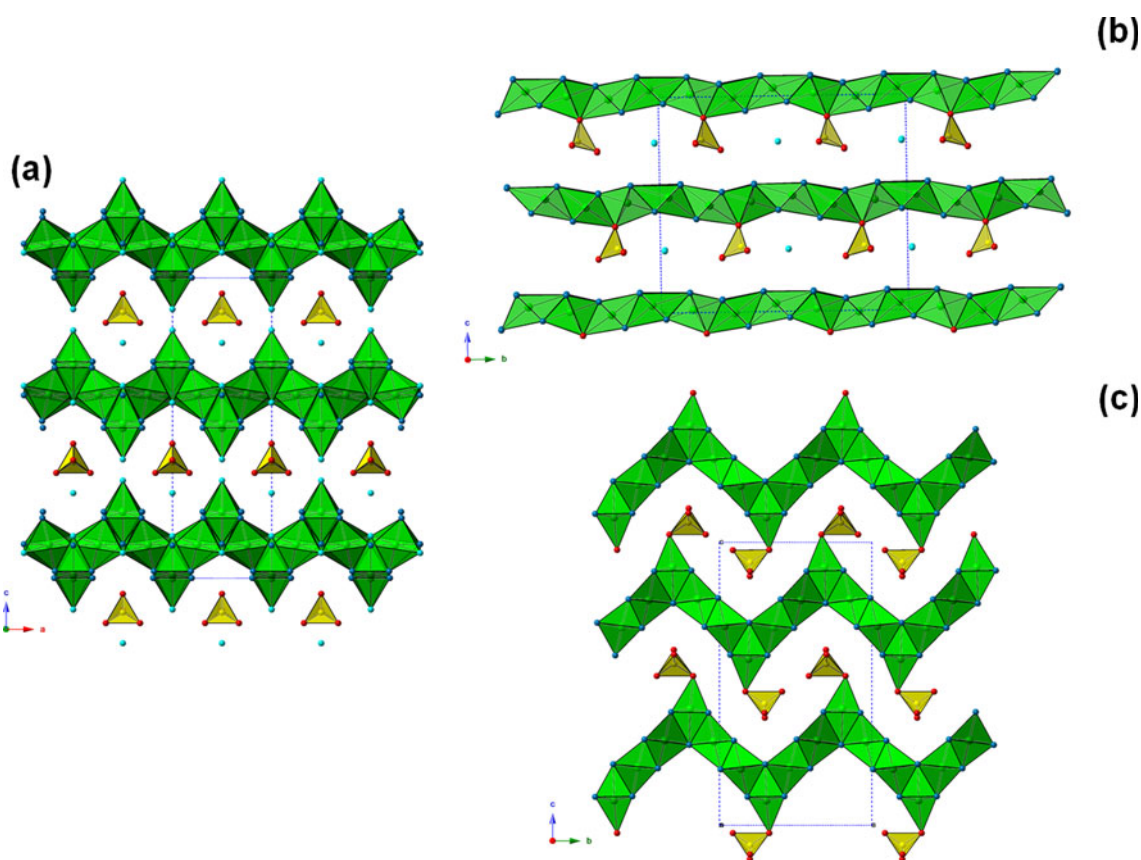
*Calculated using the relationships of Ferraris and Ivaldi (1988).

the most simple species are those having the chemical formula $\text{Cu}(\text{SO}_4)\cdot n\text{H}_2\text{O}$ ($0 < n < 7$): chalcocyanite ($n = 0$), poitevinite ($n = 1$), bonattite ($n = 3$), chalcantite ($n = 5$) and boothite ($n = 7$). Their crystal structures are reviewed by Eby and Hawthorne (1993). Chalcocyanite typically occurs in fumarolic environments. Indeed, it was first described from Vesuvius, Italy, by Scacchi (1873), along with another anhydrous copper oxy-sulfate, dolerophanite, $\text{Cu}_2\text{O}(\text{SO}_4)$. The other hydrated copper sulfates listed above are usually related to the weathering of Cu ores, although in some case they can be found also as sublimates in fumaroles (e.g. Balassone *et al.*, 2019).

The remaining species, commonly associated with weathered Cu ores (e.g. Zittlau *et al.*, 2013), are represented by the two basic copper sulfates antlerite and brochantite and seven hydrated basic copper sulfates. Isselite belongs to this latter group of copper sulfates, showing the presence of $(\text{OH})^-$ and H_2O groups. In particular, it is chemically related to redgillite, $\text{Cu}_6(\text{SO}_4)$

Table 8. Natural Cu sulfates in the system CuO–SO₃–H₂O.

Mineral	Chemical formula	<i>a</i> (Å)	<i>b</i> (Å)	<i>c</i> (Å)	α (°)	β (°)	γ (°)	Space group	Reference
Antlerite	Cu ₃ (SO ₄)(OH) ₄	8.24	6.04	11.99	90	90	90	<i>Pnma</i>	Hawthorne <i>et al.</i> (1989)
Bonattite	Cu(SO ₄)(H ₂ O) ₃	5.59	13.03	7.34	90	97.1	90	<i>Cc</i>	Zahrobsky and Baur (1966)
Boothite	Cu(SO ₄)(H ₂ O) ₆ ·H ₂ O	14.19	6.54	10.82	90	106.0	90	<i>P2₁/c</i>	Leverett <i>et al.</i> (2004)
Brochantite	Cu ₄ (SO ₄)(OH) ₆	13.14 ¹	9.86 ¹	6.02 ¹	90 ¹	103.2 ¹	90	<i>P2₁/a¹</i>	Merlino <i>et al.</i> (2003)
		12.78 ²	9.87 ²	6.03 ²	90.2 ²	90 ²	90 ²	<i>P2₁/n²</i>	
Chalcanthite	Cu(SO ₄)(H ₂ O) ₄ ·H ₂ O	6.14	10.74	5.99	82.3	107.4	102.7	<i>Pī</i>	Bacon and Titterton (1975)
Chalcocyanite	Cu(SO ₄)	8.41	6.71	4.83	90	90	90	<i>Pnma</i>	Wildner and Giester (1988)
Dolerophanite	Cu ₂ O(SO ₄)	9.37	6.32	7.64	90	122.3	90	<i>C2/m</i>	Effenberger (1985)
Isselite	Cu ₆ (SO ₄)(OH) ₁₀ (H ₂ O) ₄ ·H ₂ O	6.81	5.90	20.65	90	90	<i>Pmn2₁</i>	This work	
Kobayashevite	Cu ₅ (SO ₄) ₂ (OH) ₆ (H ₂ O) ₄	6.07	11.06	5.51	102.9	92.3	92.6	<i>Pī</i>	Pekov <i>et al.</i> (2013)
Langite	Cu ₄ (SO ₄)(OH) ₆ (H ₂ O)·H ₂ O	7.14	6.03	11.22	90	90	90	<i>Pc</i>	Gentsch and Weber (1984)
Montetrisaite	Cu ₆ (SO ₄)(OH) ₁₀ ·2H ₂ O	2.99	16.97	14.81	90	90	90	<i>Cmc2₁</i>	Orlandi and Bonaccorsi (2009)
Poitevinite	Cu(SO ₄)(H ₂ O)	5.12	5.16	7.54	107.1	107.4	92.7	<i>Pī</i>	Giester <i>et al.</i> (1994)
Posnjakite	Cu ₄ (SO ₄)(OH) ₆ (H ₂ O)	10.58	6.34	7.86	90	118.0	90	<i>Pa</i>	Mellini and Merlino (1979)
Redgillite	Cu ₆ (SO ₄)(OH) ₁₀ (H ₂ O)	3.16	10.44	19.44	90	90.1	90	<i>P2₁/c</i>	Pluth <i>et al.</i> (2005)
Wroewolfeite	Cu ₄ (SO ₄)(OH) ₆ (H ₂ O)·H ₂ O	6.04	5.65	14.34	90	93.4	90	<i>Pc</i>	Hawthorne and Groat (1985)

¹MDO₁; ²MDO₂.**Fig. 5.** Comparison between the crystal structure of isselite (a) and those of montetrisaite (b) and redgillite (c). The colour scheme is the same as in Fig. 3.

(OH)₁₀(H₂O) (Pluth *et al.*, 2005) and montetrisaite, Cu₆(SO₄)(OH)₁₀(H₂O)₂ (Orlandi and Bonaccorsi, 2009). However, notwithstanding the chemical similarities, the crystal structure of isselite is different from those shown by redgillite and montetrisaite (Fig. 5). In addition, isselite could be the Cu analogue of guarinoite, Zn₆(SO₄)(OH)₁₀·5H₂O (Sarp, 1993). However, Mills *et al.* (2019) noted that guarinoite might have been misidentified in its original description and is more likely to be Na(Zn, Co)₄(SO₄)(OH)₆Cl·5–6H₂O and equivalent to Co-rich gordaite-2H.

Nickel partitioning in isselite

After the first identification of isselite on the type specimen from the Lagoscuro mine, this mineral was identified, through powder X-ray diffraction, also on a sample from the Monte Ramazzo mine, as thin flattened acicular crystals associated with brochantite. Only EDS chemical data are available for this new occurrence; however, these data clearly indicated the occurrence of Ni, whereas Co and other elements are below the detection

limit. The Ni/(Ni + Cu) atomic ratio is close to 0.19, similar to the value observed in the type material, where the Ni/(Mg + Co + Ni + Cu + Zn) atomic ratio is 0.16. In both cases, the ideal composition is close to $\text{NiCu}_5(\text{SO}_4)(\text{OH})_{10}\cdot 5\text{H}_2\text{O}$.

The similar scattering factors of Ni ($Z = 28$) and Cu ($Z = 29$) precluded the reliable description of the distribution of Ni and Cu atoms among different cation sites. Nickel and Cu are ordered in some minerals. Gillardite and the related mineral paratacamite-(Ni), both ideally $\text{Cu}_3\text{Ni}(\text{OH})_6\text{Cl}_2$, are atacamite-group minerals where Ni is partitioned in the octahedrally coordinated sites not showing the Jahn-Teller effect, whereas Cu^{2+} is hosted at the distorted octahedrally coordinated sites (Clissold et al., 2007; Sciberras et al., 2013). Similarly, Ni^{2+} is preferentially partitioned in the less distorted octahedrally-coordinated Me2 site of the crystal structure of glaukosphaerite, $(\text{Cu},\text{Ni})_2(\text{CO}_3)(\text{OH})_2$, whereas the Me1 site shows the typical 4 + 2 distorted octahedral coordination of Cu^{2+} (Perchiazzi and Merlino, 2006). Another example is represented by hloušekite. This mineral, having the ideal formula $\text{NiCu}_4(\text{AsO}_4)_2(\text{AsO}_3\text{OH})_2(\text{H}_2\text{O})_9$, is a member of the lindackerite supergroup and Ni is hosted at a mixed (Ni,Co) site not showing the typical distortion of Cu^{2+} -centred polyhedra (Plášil et al., 2014).

In isselite, the Cu(2) and Cu(3) sites have octahedral coordinations, showing the typical (4 + 2) distortion due to the Jahn-Teller effect for Cu^{2+} . As discussed above, these sites have slightly longer equatorial bonds and shorter apical distances with respect to those reported by Eby and Hawthorne (1993) for a typical Cu^{2+} -centred octahedron. This could suggest the substitution of Cu^{2+} by Ni^{2+} at these two positions. However, as there is no certainty about the quantification of Cu-Ni site distribution, for classification purposes the Cu(2) and Cu(3) sites could be merged, as occurs in the nomenclature of other minerals (e.g. M1 + M2 + M3 in amphibole; Hawthorne et al., 2012). In accord with the IMA-CNMNC guidelines (Bosi et al., 2019), the end-member formula of isselite can be considered Ni-free. However, the actual role of Ni in stabilising this phase deserves further study.

Conclusion

Isselite is a new secondary Cu mineral showing a novel crystal structure and a complex hydrogen-bond system. Its Ni content, observed at both of its occurrences, opens the question about the role of this element in favouring the crystallisation of this new mineral species. It is likely that isselite could be more common than thought as an alteration product of Cu-Ni ores.

Along with ramazzoite (Kampf et al., 2018), isselite is the second new mineral discovered in the assemblages from the Monte Ramazzo mining complex, stressing the necessity for further investigation of this locality. In particular, a deep understanding of the geochemical relations between the Cu-Fe-Ni-Co primary mineralisation and their secondary alteration products would shed light on the possible role of hydrothermal fluids in Ni vs. Co selective mobilisation and enrichment as well as on the degree of hydrothermal alteration of the Monte-Ramazzo-Lagoscuore ore deposit.

Supplementary material. To view supplementary material for this article, please visit <https://doi.org/10.1180/mgm.2020.50>.

Acknowledgements. Marco Esposito and Fabrizio Castellaro are acknowledged for providing the first specimen of isselite and the photo used in this paper. The comments of three anonymous reviewers improved the quality of the original manuscript.

References

- Bacon G.E. and Titterton D.H. (1975) Neutron-diffraction studies of $\text{CuSO}_4\cdot 5\text{H}_2\text{O}$ and $\text{CuSO}_4\cdot 5\text{D}_2\text{O}$. *Zeitschrift für Kristallographie*, **141**, 330–341.
- Balassone G., Petti C., Mondillo N., Panikorovskii T.L., de Gennaro R., Cappelletti P., Altomare A., Corriero N., Cangiano M. and D'Orazio L. (2019) Copper minerals at Vesuvius Volcano (southern Italy): A mineralogical review. *Minerals*, **9**, 730.
- Biagioni C., Belmonte D., Carbone C., Cabella R., Zaccarini F. and Balestra C. (2019a) Arsenmedaite, $\text{Mn}_6^+\text{As}_5^{5+}\text{Si}_5\text{O}_{18}(\text{OH})$, the arsenic analogue of medaite, from the Molinello mine, Liguria, Italy: occurrence and crystal structure. *European Journal of Mineralogy*, **31**, 117–126.
- Biagioni C., Belmonte D., Carbone C., Cabella R., Demitri N., Perchiazzi N., Kampf A.R. and Bosi F. (2019b) Isselite, IMA 2018-139. CNMNC Newsletter No. 48, April 2019, page 316; *Mineralogical Magazine*, **83**, 315–317.
- Bindi L., Carbone C., Belmonte D., Cabella R. and Bracco R. (2013) Weissite from Gambatesa mine, Val Graveglia, Liguria, Italy: occurrence, composition and determination of the crystal structure. *Mineralogical Magazine*, **77**, 475–483.
- Bosi F., Hatert F., Hälenius U., Pasero M., Miyawaki R. and Mills S.J. (2019) On the application of the IMA-CNMNC dominant-valency rule to complex mineral compositions. *Mineralogical Magazine*, **83**, 627–632.
- Breese N.E. and O'Keeffe M. (1991) Bond-valence parameters for solids. *Acta Crystallographica*, **B47**, 192–197.
- Burns P.C. and Hawthorne F.C. (1996) Static and dynamic Jahn-Teller effects in Cu^{2+} -oxysalt minerals. *The Canadian Mineralogist*, **34**, 1089–1105.
- Cabella R., Lucchetti G. and Marescotti P. (1998) Mn-ores from Eastern Liguria ophiolitic sequences ("Diaspri di Monte Alpe" Formation, Northern Apennines, Italy). *Trends in Mineralogy*, **2**, 1–17.
- Capponi G. and Crispini L. (2008) *Note Illustrative alla Carta Geologica d'Italia Foglio 213–230: Genova*. APAT, Dipartimento Difesa del Suolo, Servizio Geologico d'Italia, Regione Liguria, 139 pp.
- Clissold M.E., Leverett P., Williams P.A., Hibbs D.E. and Nickel E.H. (2007) The structure of gillardite, the Ni-analogue of herbertsmithite, from Widgiemooltha, Western Australia. *The Canadian Mineralogist*, **45**, 317–320.
- Cortesogno L., Lucchetti G. and Penco A.M. (1977) Le associazioni a zeoliti, carbonati e solfuri della miniera di Campegli: un esempio di mineralizzazione in condizioni di tipo idrotermale durante le ultime fasi della tettonica alpina. *Ofoliti*, **1976** (3), 383–389.
- Eby R.K. and Hawthorne F.C. (1993) Structural relations in copper oxysalt minerals. I. Structural hierarchy. *Acta Crystallographica*, **B49**, 28–56.
- Effenberger H. (1985) $\text{Cu}_2\text{O}(\text{SO}_4)$, dolerophanite: Refinement of the crystal structure with a comparison of $[\text{OCu}(\text{II})_4]$ tetrahedra in inorganic compounds. *Monatshefte für Chemie*, **116**, 927–931.
- Ferrario A. and Garuti G. (1980) Copper deposits in the basal breccias and volcano-sedimentary sequences of the Eastern Ligurian Ophiolites (Italy). *Mineralium Deposita*, **15**, 291–303.
- Ferraris G. and Ivaldi G. (1988) Bond valence vs bond length in O...O hydrogen bonds. *Acta Crystallographica*, **B44**, 341–344.
- Frost R.L., Williams P.A., Martens W., Leverett P. and Klopogge J.T. (2004) Raman spectroscopy of basic copper (II) and some complex copper (II) sulfate minerals: Implications for hydrogen bonding. *American Mineralogist*, **89**, 1130–1137.
- Galli M. (1954) Studi petrografici sulle formazioni ofiolitiche dell'Appennino Ligure. Nota I. I diabasi di Sestri Ponente. *Periodico di Mineralogia*, **23**, 73–99.
- Galli M. (1963) Studi petrografici sulla formazione ofiolitica dell'Appennino Ligure. Nota V. Le rocce peridotitico-serpentinose. *Periodico di Mineralogia*, **32**, 575–621.
- Gentsch M. and Weber K. (1984) Structure of langite, $\text{Cu}_4[(\text{OH})_6|\text{SO}_4]\cdot 2\text{H}_2\text{O}$. *Acta Crystallographica*, **C40**, 1309–1311.
- Gierster G., Lengauer C.L. and Redhammer G. (1994) Characterization of the $\text{FeSO}_4\cdot \text{H}_2\text{O}$ - $\text{Cu}(\text{SO}_4)\cdot \text{H}_2\text{O}$ solid-solution series, and the nature of poitevinite, $(\text{Cu},\text{Fe})\text{SO}_4\cdot \text{H}_2\text{O}$. *The Canadian Mineralogist*, **32**, 873–884.
- Gunter M.E., Bandli B.R., Bloss F.D., Evans S.H., Su S.C. and Weaver R. (2004) Results from a McCrone spindle stage short course, a new version of EXCALIBUR, and how to build a spindle stage. *The Microscope*, **52**, 23–39.

- Hawthorne F.C. and Groat L.A. (1985) The crystal structure of wroewolfeite, a mineral with $[\text{Cu}_4(\text{OH})_6(\text{SO}_4)(\text{H}_2\text{O})]$ sheets. *American Mineralogist*, **70**, 1050–1055.
- Hawthorne F.C., Groat L.A., and Eby R.K. (1989) Antlerite, $\text{Cu}_3\text{SO}_4(\text{OH})_4$, a heteropolyhedral wallpaper structure. *The Canadian Mineralogist*, **27**, 205–209.
- Hawthorne F.C., Oberti R., Harlow G.E., Maresch W.V., Martin R.F., Schumacher J.C. and Welch M.D. (2012) Nomenclature of the amphibole supergroup. *American Mineralogist*, **97**, 2031–2048.
- Holland T.J.B. and Redfern S.A.T. (1997) Unit cell refinement from powder diffraction data: the use of regression diagnostics. *Mineralogical Magazine*, **61**, 65–77.
- Issel A. (1892) *Liguria Geologica e Preistorica*. Donath Editore, Genova, Italy.
- Kabsch W. (2010) Integration, scaling, space-group assignment and post-refinement. *Acta Crystallographica*, **D66**, 125–132.
- Kampf A.R., Roberts A.C., Venance K.E., Carbone C., Belmonte D., Dunning G.E. and Walstrom R.E. (2013) Cerchiarite-(Fe) and cerchiarite-(Al), two new barium cyclosilicate chlorides from Italy and California, USA. *Mineralogical Magazine*, **77**, 69–80.
- Kampf A.R., Rossman G.R., Ma C., Belmonte D., Biagioni C., Castellaro F. and Chiappino L. (2018) Ramazzoite, $[\text{Mg}_8\text{Cu}_{12}(\text{PO}_4)(\text{CO}_3)_4(\text{OH})_{24}(\text{H}_2\text{O})_{20}] [(\text{H}_{0.33}\text{SO}_4)_3(\text{H}_2\text{O})_{36}]$, the first mineral with a polyoxometalate cation. *European Journal of Mineralogy*, **30**, 827–834.
- Kraus W. and Nolze G. (1996) POWDER CELL – a program for the representation and manipulation of crystal structures and calculation of the resulting X-ray powder patterns. *Journal of Applied Crystallography*, **29**, 301–303.
- Kolesov B.A. (2006) Raman spectra of single H_2O molecules isolated in cavities of crystals. *Journal of Structural Chemistry*, **47**, 21–34.
- Kolitsch U., Merlino S., Belmonte D., Carbone C., Cabella R., Lucchetti G. and Ciriotti M.E. (2018) Lavinskyite-1M, $\text{K}(\text{LiCu})\text{Cu}_6(\text{Si}_4\text{O}_{11})_2(\text{OH})_4$, the monoclinic MDO equivalent of lavinskyite-2O (formerly lavinskyite), from the Cerchiar manganese mine, Liguria, Italy. *European Journal of Mineralogy*, **30**, 811–820.
- Lausi A., Polentarutti M., Onesti S., Plaisier J.R., Busetto E., Bais G., Barba L., Cassetta A., Campi G., Lamba D., Pifferi A., Mande S.C., Sarma D.D., Sharma S.M. and Paolucci G. (2015) Status of the crystallography beamlines at Elettra. *The European Physical Journal Plus*, **130**, 43–51.
- Leverett P., McKinnon A.R. and Williams P.A. (2004) New data for boothite, $\text{CuSO}_4 \cdot 7\text{H}_2\text{O}$, from Burruga, New South Wales. *Australian Journal of Mineralogy*, **10**, 3–6.
- Mandarino J.A. (1979) The Gladstone–Dale relationship. Part III. Some general applications. *The Canadian Mineralogist*, **17**, 71–76.
- Mandarino J.A. (1981) The Gladstone–Dale relationship. Part IV. The compatibility concept and its application. *The Canadian Mineralogist*, **19**, 441–450.
- Mellini M. and Merlino S. (1979) Posnjakite: ${}^{\infty}[\text{Cu}_4(\text{OH})_6(\text{H}_2\text{O})\text{O}]$ octahedral sheets in its structure. *Zeitschrift für Kristallographie*, **149**, 249–257.
- Merlino S., Perchiazzi N. and Franco E. (2003) Brochantite, $\text{Cu}_4(\text{SO}_4)(\text{OH})_6$: OD character, polytypism and crystal structures. *European Journal of Mineralogy*, **15**, 267–275.
- Mills S., Missen O. and Favreau G. (2019) The crystal structure of Ni-rich gordaite-théresémagnanite from Cap Garonne, France. *Mineralogical Magazine*, **83**, 459–463.
- Moroni M., Rossetti P., Naitza S., Magnani L., Ruggieri G., Aquino A., Tartarotti P., Franklin A., Ferrari E., Castelli D., Oggiano G. and Secchi F. (2019) Factors controlling hydrothermal nickel and cobalt mineralization – Some suggestions from historical or deposits in Italy. *Minerals*, **9**, 429.
- Orlandi P. and Bonaccorsi E. (2009) Montetrisaite, a new hydroxy-hydrated copper sulfate species from Monte Trisa, Vicenza, Italy. *The Canadian Mineralogist*, **47**, 143–151.
- Pekov I.V., Zubkova N.V., Yapaskurt V.O., Belakovskiy D.I., Chukanov N.V., Kasatkin A.V., Kuznetsov A.M. and Pushcharovsky D.Y. (2013) Kobyashevite, $\text{Cu}_5(\text{SO}_4)_2(\text{OH})_6 \cdot 4\text{H}_2\text{O}$, a new devilline-group mineral from the Vishnevye Mountains, South Urals, Russia. *Mineralogy and Petrology*, **107**, 201–210.
- Perchiazzi N. and Merlino S. (2006) The malachite-rosasite group: crystal structures of glaukosphaerite and pokrovskite. *European Journal of Mineralogy*, **18**, 787–792.
- Pipino G. (1977) L'antica miniera di Monte Ramazzo presso Genova e i suoi minerali. *Rivista Mineralogica Italiana*, **8**, 61–73.
- Plášil J., Sejkora J., Škoda R., Novák M., Kasatkin A.V., Škacha P., Veselovský F., Fejfarová K. and Ondruš P. (2014) Hloušekite, $(\text{Ni},\text{Co})\text{Cu}_4(\text{AsO}_4)_2(\text{AsO}_3\text{OH})_2(\text{H}_2\text{O})_9$, a new member of the lindackerite supergroup from Jáchymov, Czech Republic. *Mineralogical Magazine*, **78**, 1341–1353.
- Pluth J.J., Steele I.M., Kampf A.R. and Green D.I. (2005) Redgillite, $\text{Cu}_6(\text{OH})_{10}(\text{SO}_4) \cdot \text{H}_2\text{O}$, a new mineral from Caldbeck Fells, Cumbria, England: description and crystal structure. *Mineralogical Magazine*, **69**, 973–980.
- Rolandi V. (1974) *I giacimenti cupriferi di Molini, Monte Ramazzo e Sassello nel Gruppo di Voltri*. MSc Thesis (unpublished), University of Milan, Italy, 111 pp.
- Sarp H. (1993) Guarinoite $(\text{Zn},\text{Co},\text{Ni})_6(\text{SO}_4)(\text{OH},\text{Cl})_{10} \cdot 5\text{H}_2\text{O}$ et therese-magnanite $(\text{Co},\text{Zn},\text{Ni})(\text{SO}_4)(\text{OH},\text{Cl})_{10} \cdot 8\text{H}_2\text{O}$, deux nouveaux minéraux de la mine de Cap Garonne, Var, France. *Archives des Sciences, Genève* **46**, 37–44.
- Scacchi A. (1873) Nuove specie di solfati di rame. Idrociano. *Atti dell'Accademia delle Scienze Fisiche e Matematiche*, **5**, 26–29.
- Schwarzenbach E.M., Früh-Green G.L., Bernasconi S.M., Alt J.C., Shanks III W.C., Gaggero L. and Crispini L. (2012) Sulfur geochemistry of peridotite-hosted hydrothermal systems: comparing the Ligurian ophiolites with oceanic serpentinites. *Geochimica et Cosmochimica Acta*, **91**, 283–305.
- Sciberras M.J., Leverett P., Williams P.A., Hibbs D.E., Downes P.J., Welch M.D. and Kampf A.R. (2013) Paratacamite-(Ni), $\text{Cu}_3(\text{Ni},\text{Cu})\text{Cl}_2(\text{OH})_6$, a new mineral from the Carr Boyd Rocks mine, Western Australia. *Australian Journal of Mineralogy*, **17**, 39–44.
- Sheldrick G.M. (1997) SHELXS97 and SHELXL97. Program for Crystal Structure Solution and Refinement. University of Göttingen, Göttingen, Germany.
- Sheldrick G.M. (2015) Crystal structure refinement with SHELXL. *Acta Crystallographica*, **C71**, 3–8.
- Tenailleau C., Pring A., Etschmann B., Brugger J., Grguric B. and Putnis A. (2006) Transformation of pentlandite to violarite under mild hydrothermal conditions. *American Mineralogist*, **91**, 706–709.
- Wildner M. and Giester G. (1988) Crystal structure refinements of synthetic chalcocyanite (CuSO_4) and zincosite (ZnSO_4). *Mineralogy and Petrology*, **39**, 201–209.
- Wilson A.J.C., Ed. (1992) *International Tables for Crystallography, Volume C: Mathematical, physical and chemical tables*. Kluwer Academic, Dordrecht, The Netherlands.
- Xia F., Brugger J., Chen G., Ngothai Y., O'Neill B., Putnis A. and Pring A. (2009) Mechanism and kinetics of pseudomorphic mineral replacement reactions: A case study of the replacement of pentlandite by violarite. *Geochimica et Cosmochimica Acta*, **73**, 1945–1969.
- Zaccarini F. and Garuti G. (2008) Mineralogy and chemical composition of VMS deposits of northern Apennine ophiolites, Italy: evidence for the influence of country rock type on ore composition. *Mineralogy and Petrology*, **94**, 61–83.
- Zahrobsky R. and Baur W.H. (1966) The crystal structure of copper (II) sulfate trihydrate. *American Mineralogist*, **51**, 276–276.
- Zittlau A.H., Shi Q., Boerio-Gates J., Woodfield B.F. and Majzlan J. (2013) Thermodynamics of the basic copper sulfates antlerite, posnjakite, and brochantite. *Chemie der Erde*, **73**, 39–50.